A X-ray photoelectron spectroscopy study of HDTMAB distribution within organoclays

Hongping He [a,b,*], Qin Zhou [a,c], Ray L. Frost [b], Barry J. Wood [d],
Loc V. Duong [b], J. Theo Kloprogge [b,*]

[a] *Guangzhou Institute of Geochemistry, Chinese Academy of Sciences, Guangzhou 510640, China*
[b] *Inorganic Materials Research Program, School of Physical and Chemical Sciences, Queensland University of Technology,*
GPO Box 2434, Brisbane, Qld 4001, Australia
[c] *Graduate University of the Chinese Academy of Sciences, Beijing 100039, China*
[d] *Brisbane Surface Analysis Facility, University of Queensland, Brisbane, Qld 4072, Australia*

Abstract

X-ray photoelectron spectroscopy (XPS) in combination with X-ray diffraction (XRD) and high-resolution thermogravimetric analysis (HRTG) has been used to investigate the surfactant distribution within the organoclays prepared at different surfactant concentrations. This study demonstrates that the surfactant distribution within the organoclays depends strongly on the surfactant loadings. In the organoclays prepared at relative low surfactant concentrations, the surfactant cations mainly locate in the clay interlayer, whereas the surfactants occupy both the clay interlayer space and the interparticle pores in the organoclays prepared at high surfactant concentrations. This is in accordance with the dramatic pore volume decrease of organoclays compared to those of starting clays. XPS survey scans show that, at low surfactant concentration (<1.0 CEC), the ion exchange between Na^+ and $HDTMA^+$ is dominant, whereas both cations and ion pairs occur in the organoclays prepared at high concentrations (>1.0 CEC). High-resolution XPS spectra show that the modification of clay with surfactants has prominent influences on the binding energies of the atoms in both clays and surfactants, and nitrogen is the most sensitive to the surfactant distribution within the organoclays.
© 2006 Elsevier B.V. All rights reserved.

Keywords: X-ray photoelectron spectroscopy; X-ray diffraction; Organoclay; Surfactant distribution; Surfactant loading

1. Introduction

Organoclays represent a family of materials with hydrophobic surfaces, synthesized by modifying swelling clays with various surfactants. During the last 50 years, organoclays have attracted great interest in a number of applications, such as adsorbents for organic pollutants [1–4], rheological control agents [5], reinforcing fillers for plastics [6], clay-based nanocomposites [7], and precursors for preparing mesoporous materials [8,9].

Up to now, a large variety of organoclays have been synthesized using different surfactants [1–4,10–12] and their structures have been characterized using various techniques, including X-ray diffraction (XRD) [11,12], Fourier transform infrared spectroscopy (FT-IR) [13–15], Raman spectroscopy [16], thermogravimetric measurement (TG) [17–21], magic angle spinning nuclear magnetic resonance (MAS NMR) [22,23] and transmission electron microscopy (TEM) [24–26]. In these cases, the detailed information about the interlayer structure, the conformation of the intercalated surfactant and thermal stability of the resultant organoclays rather than the surface characteristics was obtained. However, in various applications of organoclays, the surface characteristics of the resultant organoclays is of high importance since the affinity between the organoclays and the matrix depends strongly on the surface characteristics of the organoclays. Unfortunately, the aforementioned techniques provide little information about the surface characteristics of the organoclays.

X-ray photoelectron spectroscopy (XPS) has been demonstrated to be a powerful technique to investigate the surface characteristics of various materials, including clay minerals and

---

* Corresponding authors.
  E-mail addresses: hehp@gig.ac.cn (H. He), t.kloprogge@qut.edu.au (J.T. Kloprogge).

related products [27–30]. XPS can provide elemental analysis for essentially the entire periodic table. Because the electrons whose energies are analyzed arise from a depth of no greater than about 2–5 nm, the technique is surface-sensitive and suitable to investigate the surface characteristics of clays and the resultant organoclays.

With the increase of applications in various fields, the study of organoclay surface characteristics will attract great interest. Zhu and co-workers [24] proposed that the various sorption mechanisms of organoclays for pollutants might result from the different distributions of surfactant within the organoclays. Recently, our study demonstrated that washing the organoclays with solvents resulted in the change of surface energy of the resultant organoclays, resulting from the removal of physically adsorbed surfactant [31]. Both of the abovementioned cases suggest that the distribution of surfactant have a significant effect on the surface property of the organoclays and a consequent influence on their applications.

Unfortunately, to date, there is no publication available on XPS of organoclays, which can provide convincing evidence about the distribution of surfactant within organoclays. The objective of this report is to determine the surfactant distribution within the organoclays using XPS, in conjunction with X-ray diffraction (XRD) and high-resolution thermogravimetric analysis (HRTG). This study demonstrates that the distribution of surfactant (in the interlayer space and outside clay layer) depends strongly on the surfactant loading within organoclays and N 1s spectra are most sensitive to the surfactant distribution. This is of high importance to well understand the microstructure of organoclays and for their applications.

2. Experimental

2.1. Materials

Ca-montmorillonite (Ca-Mt) was obtained from Hebei, China. The sample was purified by sedimentation and the $<2\,\mu m$ fraction was collected and dried at $90\,^\circ C$. The sample was ground through a 200 mesh sieve and sealed in a glass tube for use. Its cation exchange capacity (CEC) is 90.8 mequiv./100 g, determined by NH_4^+ method as described in the literature [32]. Its chemical formula can be expressed as $Ca_{0.19}Mg_{0.06}Na_{0.01}$ $(Si_{3.96}Al_{0.04})(Al_{1.44}Fe_{0.09}Mg_{0.47})O_{10}(OH)_2 \cdot nH_2O$, calculated from the chemical analysis result. The surfactant used in this study is hexadecyltrimethylammonium bromide (HDTMAB) with a purity of 99%, provided by YuanJu Chem. Co. Ltd., China.

2.2. Preparation of organoclays

Before synthesis of $HDTMA^+$ intercalated montmorillonites, sodium-montmorillonite (Na-Mt) was prepared from Ca-Mt as follows: 10 g of the mixture of Ca-Mt and Na_2CO_3 in the ratio of 94:6 was added into 100 ml of deionized water and stirred at $80\,^\circ C$ for 3 h. During the stirring, several drops of HCl were added into the suspension to dissolve the CO_3^{2-}. Na-Mt was collected by centrifugation and washed with deionized water until the solution was free of chloride (titration with $AgNO_3$).

The Na-Mt was dried at $105\,^\circ C$, ground through a 200 mesh sieve and kept in a sealed bottle.

The syntheses of $HDTMA^+$ intercalated montmorillonites were performed by the following procedure: 2.5 g of Na-montmorillonite was first dispersed in 300 ml of deionized water and then a desired amount of HDTMAB was slowly added. The added surfactant varied from 0.5 to 2.5 CEC of montmorillonite. The reaction mixtures were stirred in a water bath for 9 h at $80\,^\circ C$. All products were washed free of bromide anions (titration with $AgNO_3$), dried at $60\,^\circ C$ and ground in an agate mortar to pass through a 200 mesh sieve. The organoclay prepared at the surfactant concentration of 0.5 CEC was denoted as 0.5 CEC-Mt and the others were marked in the same way.

2.3. Characterization

X-ray diffraction (XRD) patterns of the samples were recorded between 1.5° and 20° (2θ) at a scanning speed of 2°/min, using Rigaku D/max-1200 diffractometer with Cu Kα radiation (30 mA and 40 kV).

High-resolution thermogravimetric analysis (HRTG) was performed on a TA Instruments Inc. Q500 thermobalance. Samples were heated from room temperature to $1000\,^\circ C$ at a heating rate of $10\,^\circ C$/min with a resolution of $6\,^\circ C$ under N_2 atmosphere ($80\,cm^3$/min). Approximately 30 mg of finely ground sample was heated in an open platinum crucible.

N_2 adsorption–desorption isotherms were gained at liquid nitrogen temperature with a Micromeritics ASAP 2010 gas sorption analyzer (Quantachrome Co., USA). Before measurement, the samples were pre-heated at $80\,^\circ C$ under N_2 for ca. 24 h. The specific surface area was calculated by the BET equation and the total pore volumes were evaluated from nitrogen uptake at relative pressure of ca. 0.99.

The X-ray photoelectron spectroscopy (XPS) analyses were performed on a Kratos AXIS Ultra with a monochromatic Al X-ray source at 150 W. Each analysis started with a survey scan from 0 to 1200 eV with a dwell time of 100 ms, pass energy of 160 eV at steps of 1 eV with one sweep. For the high-resolution analysis, the number of sweeps was increased, the pass energy was lowered to 20 eV at steps of 100 meV and the dwell time was changed to 250 ms. Band component analyses were undertaken using the Jandel 'Peakfit' software package, which enabled the type of fitting function to be selected and allows specific parameters to be fixed or varied accordingly. Band fitting was done using a Lorenz–Gauss cross-product function with the minimum number of component bands used for the fitting process [33].

3. Results and discussion

3.1. X-ray diffraction (XRD)

Fig. 1 shows the XRD patterns of montmorillonites and the organoclays. The basal spacing of Na-Mt is 1.24 nm, which is a characteristic d value for Na-montmorillonite. However, after modification with surfactant, the interlayer height of montmorillonite is obviously increased. With an increase of surfactant concentration in the preparation solution, the basal spac-
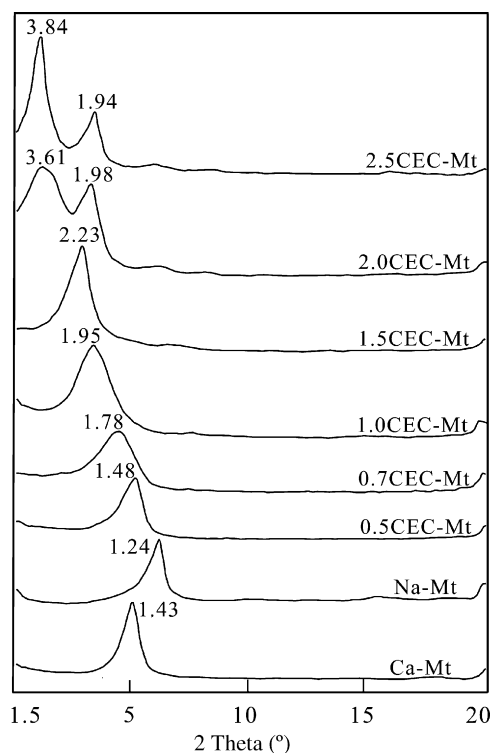
Fig. 1. XRD patterns of montmorillonite and the resultant organoclays.

ings of the resultant organoclays increase in the following order: 1.24 nm (Na-Mt) → 1.48 nm (0.5 CEC-Mt) → 1.78 nm (0.7 CEC-Mt) → 1.95 nm (1.0 CEC-Mt) → 2.23 nm (1.5 CEC-Mt) → 3.61 nm (2.0 CEC-Mt) → 3.84 nm (2.5 CEC-Mt). Here, it can be understood that there are five different surfactant arrangements adopted within the montmorillonite interlayer space, i.e. lateral monolayer in 0.5 CEC-Mt, lateral bilayer in 0.7 CEC-Mt, pseudotrilayer in 1.0 CEC-Mt, paraffin monolayer in 1.5 CEC-Mt and paraffin bilayer in 2.0 and 2.5 CEC-Mt, respectively, in agreement with previous experimental and molecular modeling reports [11,12,34–36]. Fig. 2(I) is the schematics of the organoclays with different surfactant arrangement models.

3.2. XPS characterization

Fig. 3 displays the XPS survey scans of HDTMAB, Na-Mt and the representative organoclays (0.7 and 2.5 CEC-Mt). The XPS results clearly show that the presences of carbon, nitrogen and bromine in HDTMAB and sodium, aluminum, silicon, oxygen, magnesium and iron in Na-Mt. The XPS result is in an excellent agreement with our chemical analysis result of montmorillonite. In addition, there is a minor amount of oxygen in HDTMAB and carbon in Na-Mt, resulting from adsorbed CO_2 [37]. The XPS survey scans show the presence of calcium in Ca-Mt (not shown), whereas in Na-Mt only sodium was observed (Fig. 3), indicating that the preparation of sodium-montmorillonite from calcium-montmorillonite in this study was successful.

The ratios of the elemental atomic concentrations in montmorillonite and the resultant organoclays are summarized

in Table 1, deduced from the corresponding XPS analyses. This calculation shows that the content of surfactant within the organoclays increases in the order of 0.5 CEC-Mt → 0.7 CEC-Mt → 1.0 CEC-Mt → 1.5 CEC-Mt → 2.0 CEC-Mt → 2.5 CEC-Mt. This is in accordance with our previous studies using other techniques and the reports in the literature [11–25]. Meanwhile, the Al/Si ratio deduced from the XPS analysis (0.36) is in good agreement with the chemical analysis (0.37). However, the Al/Si ratio in the resultant organoclays decreases with the intercalation of surfactant as shown in Table 1. This results from the increase of the interlayer distance with the intercalation of surfactant, which leads to a decreasing possibility for detecting the Al–O(OH) octahedral sheets sandwiched between the two Si–O tetrahedral sheets of the montmorillonite.

In the XPS survey scans of the organoclays, prominent peaks corresponding to magnesium and a trace of iron are always recorded, whereas that of sodium disappears. This reflects that both magnesium and iron are in the montmorillonite structure rather than in the interlayer. This is in agreement with our formula calculation. Meanwhile, the disappearance of the peak corresponding to sodium results from the exchange of sodium ions by surfactant cations.

There is no peak corresponding to bromine recorded in the XPS survey scans of 0.5, 0.7 and 1.0 CEC-Mt, whereas it is recorded in the XPS scans of 1.5, 2.0 and 2.5 CEC-Mt. The surfactant contents (in term of CEC) in the resultant organoclays, deduced from the thermogravimetric measurements (not shown), are shown in Table 1. Our calculation indicates that there is more than 1 CEC of surfactant in 1.5, 2.0 and 2.5 CEC-Mt. Here, it can be understood that, at relative low surfactant concentration (≤1 CEC in the present case), the intercalation is dominant and the surfactants enter into the clay interlayer space as cations. On the other hand, the surfactants exist within the organoclays in both formats of cations and molecules when the loaded surfactants are more than 1 CEC [38]. This concept is further supported by the high-resolution XPS scans.

3.3. High-resolution XPS

3.3.1. C 1s spectra

The C 1s spectrum of HDTMAB is characterized by two transitions centered at 284.7 and 285.7 eV, corresponding to the C–C bond in the long chain and C–N, respectively (Fig. 4). The C 1s spectra of organoclays show a significant broadening with slight changes in binding energy, indicating more than one type of surfactant–clay interaction. The change trends of binding energy for C–C and C–N as function of CEC are different as shown in Fig. 5. For the spectra corresponding to C–C, there is a significant binding energy decrease from HDTMAB to 0.5 CEC-Mt and the binding energies for 0.7 and 1.0 CEC-Mt are similar to that of 0.5 CEC-Mt. However, there is a significant increase from 1.0 to 1.5 CEC-Mt, then to 2.0 CEC-Mt and finally to 2.5 CEC-Mt. The C 1s binding energies of 2.0 and 2.5 CEC-Mt are higher than that of HDTMAB. However, the C 1s binding energies of the resultant organoclays, corresponding to the C–N bond, are similar. Here, the C 1s spectra of organoclays show that the local molecular environment of the surfactant has a promi-
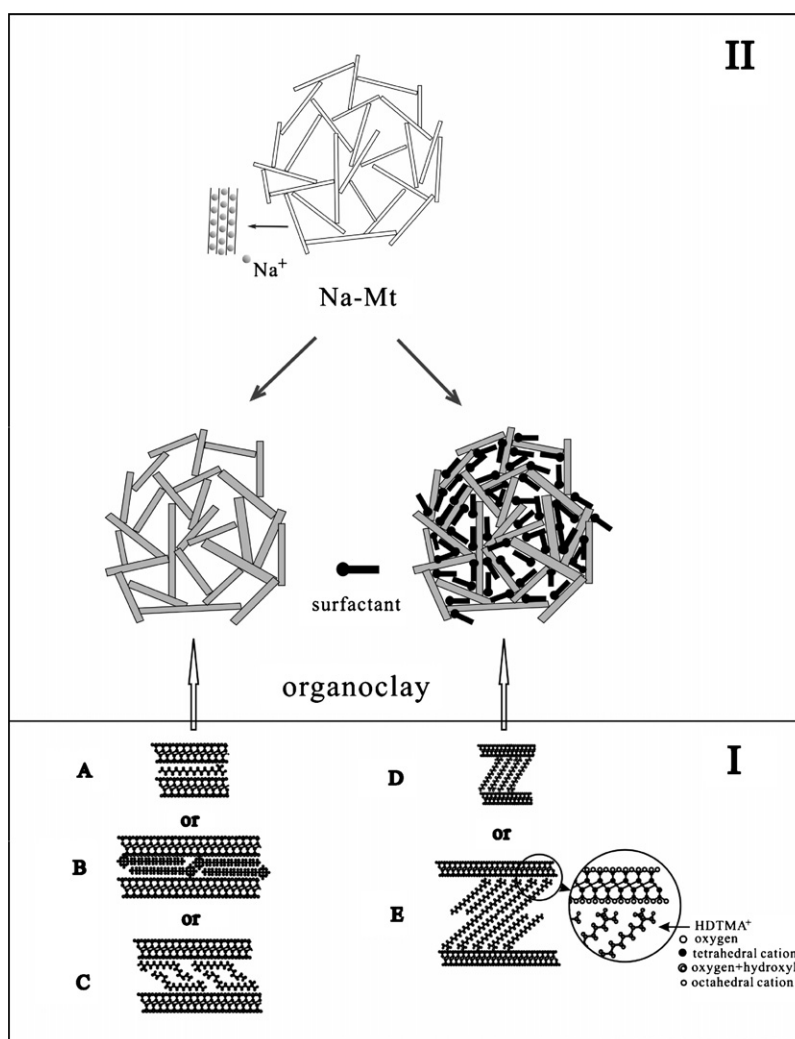
Fig. 2. The schematics of organoclays with different arrangements (I) and the schematics of Na-Mt and the resultant organoclays (II). (A) lateral monolayer; (B) lateral bilayer; (C) pseudotrilayer; (D) paraffin monolayer; (E) paraffin bilayer.

nent effect on the binding energy. Molecular modeling [34–36] demonstrates that in all arrangements of surfactant within the clay interlayer, the headgroups (nitrogen) of the alkyl chains will be close to the clay surface due to the strong electrostatic interaction between the negative clay surface and the positive headgroups of the alkyl chains. This can well explain the sim-

ilar binding energy of C 1s in C–N for the organoclays with different surfactant arrangements.

Previous reports [13–16,34–36] have shown that, in the organoclays with lower surfactant packing density, the alkyl chains within the interlayer space are parallel within the interlayer space and are individually separated. In this case, the repul-

Table 1
Surfactant loadings and the ratios of atomic concentrations in montmorillonite and the resultant organoclays based on TG and XPS analyses

Sample	Na-Mt	0.5 CEC-Mt	0.7 CEC-Mt	1.0 CEC-Mt	1.5 CEC-Mt	2.0 CEC-Mt	2.5 CEC-Mt
SL[a] (%)	–	9.73	16.73	22.13	28.19	38.73	44.17
SL[b] (vs. CEC)	–	0.33	0.61	0.86	1.19	1.9	2.4
C/Si[c]	–	2.08	2.28	2.69	3.41	5.79	6.58
Al/Si[d]	0.36	0.34	0.32	0.33	0.33	0.28	0.30
V_P (cm^3/g)	0.107	0.061	0.060	0.056	0.037	0.011	0.007

V_P: pore volume determined by BJH method from N_2 desorption isotherm.
[a] Surfactant loading within the corresponding organoclay, evaluated from high-resolution thermogravimetric analysis.
[b] Surfactant loading expressed in CEC of montmorillonite (100 g).
[c] The ratios of carbon and silicon atomic concentrations in the organoclays.
[d] The ratios of aluminum and silicon atomic concentrations in Na-montmorillonite and the organoclays.
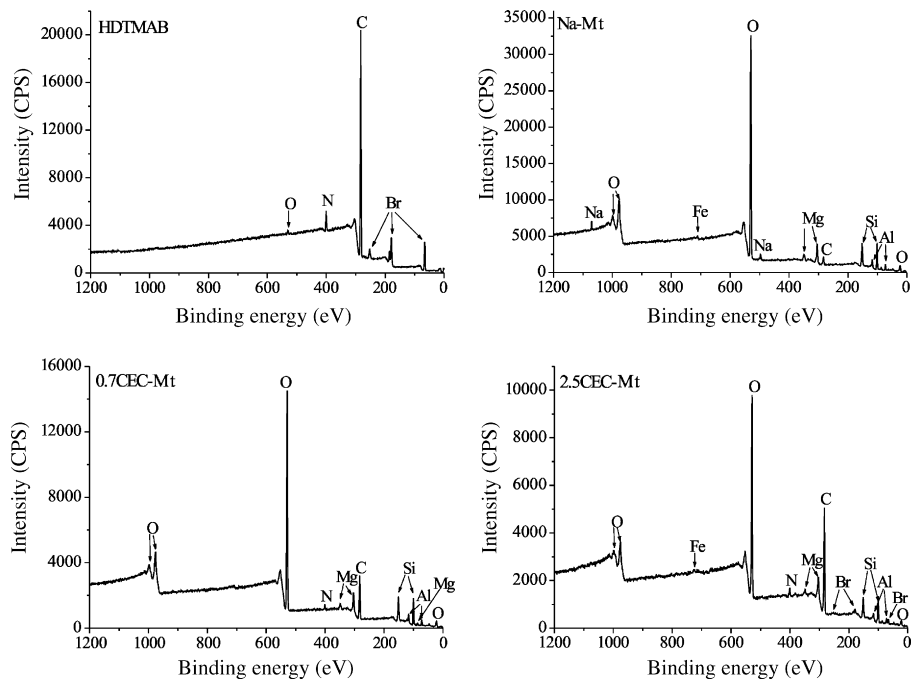
Fig. 3. XPS survey scans of HDTMAB, Ca-Mt, Na-Mt and the representative organoclays.
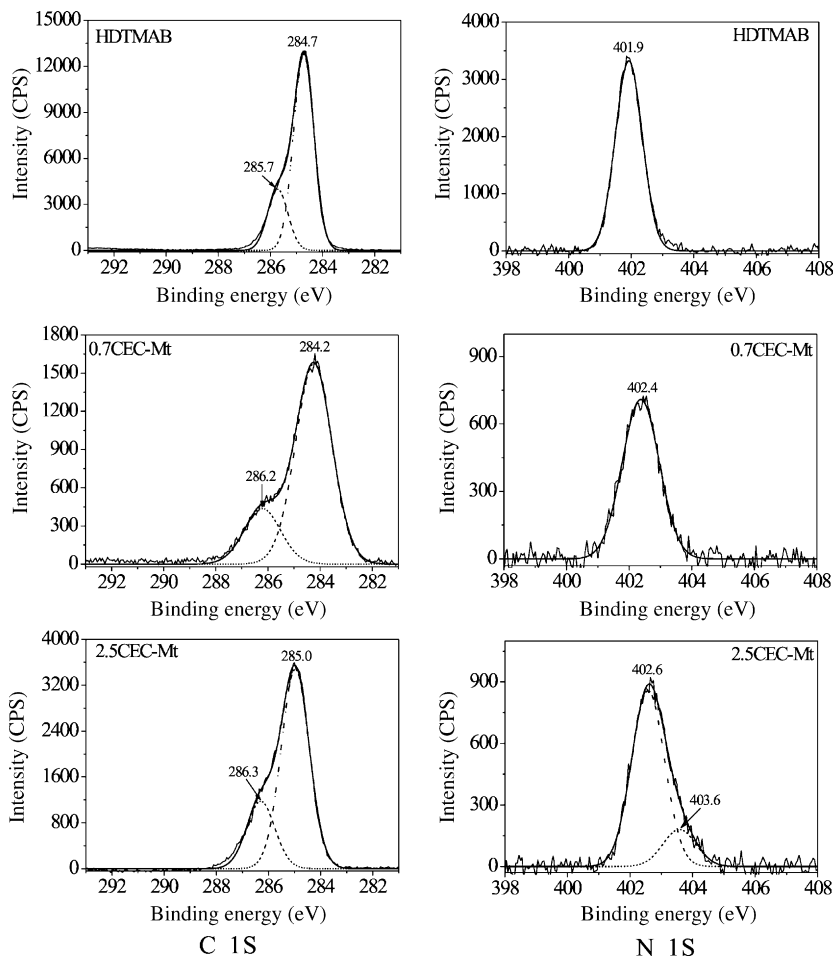

C 1S

N 1S

Fig. 4. C 1s and N 1s high-resolution XPS spectra of HDTMAB and the representative organoclays. Thin solid line, experimental curve; thick solid line, deconvolution curve; dash line, fitting curve.
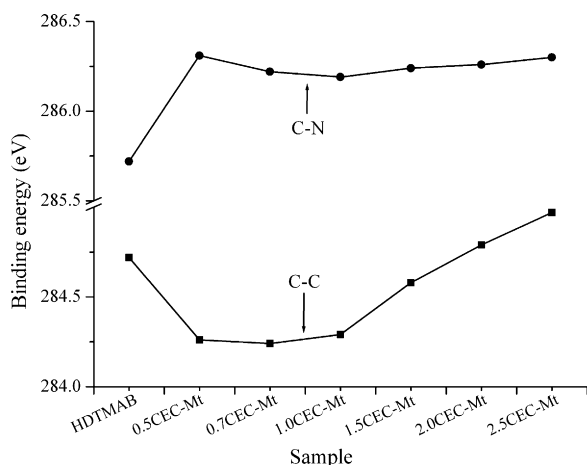
Fig. 5. The C 1s binding energy change of C–C and C–N in the resultant organoclays.

surfactant outside the clay layers. This assumption is supported by the pore volume analyses of these samples.

The nitrogen adsorption–desorption isotherms of Na-Mt and the resultant organoclays show that there are "ink-bottle" like pores in these clays, which could be described as a "house of cards" structure [40,41]. Meanwhile, the pore volumes of these samples (Table 1) show that there is a dramatic decreases of pore volumes from Na-Mt to 0.5 CEC-Mt, followed by a smooth decrease till 1.0 CEC-Mt, then a more pronounced decrease till 2.0 CEC-Mt. The dramatic pore volume decrease of the organoclays with less than 1 CEC can be explained as the intercalation of the HDTMA$^+$ cations into the clay interlayer space. And the significant pore volume decrease from 1.0 CEC-Mt to the organoclays with a surfactant loading more than 1 CEC is resulted from the occupation of surfactant in the interparticle pores. This

sive interaction between the hydrocarbon chain–silicate surface is dominant, whereas the interaction among the hydrocarbon chains is very weak. The local environment of the intercalated surfactant is absolutely different from those in bulk state. With the increase of surfactant packing density, the interchain interaction among the surfactants becomes the dominant force and the orientation of the hydrocarbon tail changes from parallel to the silicate surface within the interlayer space to parallel but at an angle to the silicate surface as shown by XRD and FT-IR results [11–15]. The interaction among alkyl chains will increase with the increase of the surfactant packing density [11,12,21] and this will result in the ordered packing of the alkyl chains as indicated by FT-IR and Raman spectroscopy [13–16]. The local environment of the surfactant within the resultant organoclays strongly depends on their loaded amounts, resulting in a variation of the C 1s binding energy of the C–C bond in the alkyl chains.

3.3.2. N 1s spectra

The high-resolution scans of nitrogen in HDTMAB and the representative organoclays are displayed in Fig. 4. For HDTMAB, a single 1s transition is observed with a binding energy of 401.9 eV, which is similar to that reported in a previous study [39]. The high-resolution scans of nitrogen in 0.5, 0.7 and 1.0 CEC-Mt shows a single 1s transition with a slight increase of the binding energy (ca. 0.5 eV) and full-width-at-half-maximum (FWHM), indicating the local environment of the intercalated surfactant is different from that in bulk state. This is in accordance with the conclusion deduced from the C 1s spectra.

However, the nitrogen high-resolution scans of organoclays with a surfactant loading more than 1 CEC show two overlapping bands related to two different N 1s transitions. The N 1s spectrum of 2.5 CEC-Mt is shown in Fig. 4, containing two bands at ca. 403.6 and 402.6 eV, respectively, reflecting two different local environments for the surfactant within the organoclay. The band with a binding energy (402.6 eV) similar to that in 0.5, 0.7 and 1.0 CEC-Mt, should be attributed to the intercalated surfactant while the other one (ca. 403.6 eV) should be attributed to the
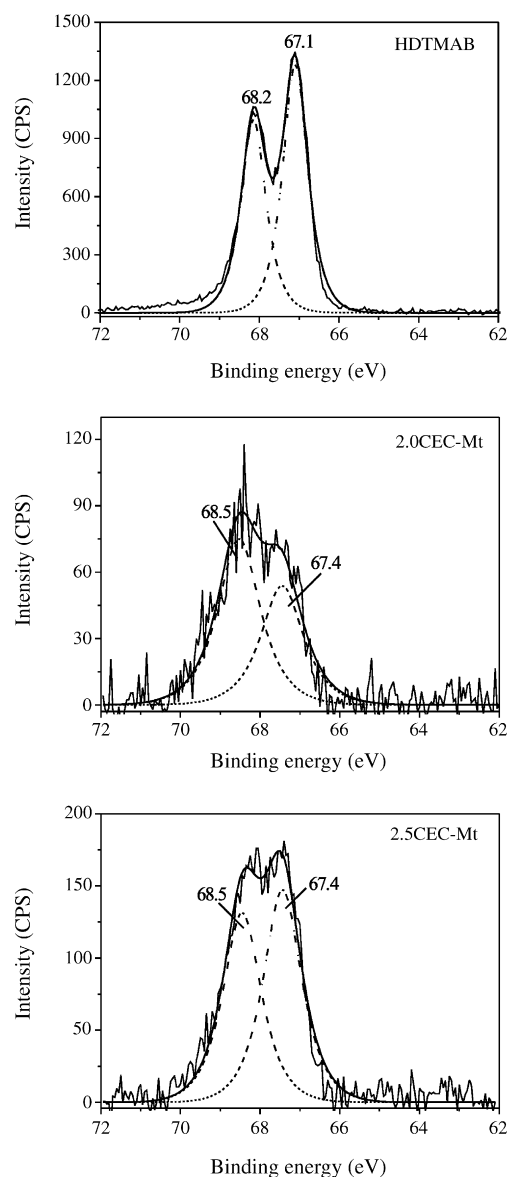

Fig. 6. Br 3d high-resolution XPS spectra of HDTMAB, 2.0 and 2.5 CEC-Mt. Thin solid line, experimental curve; thick solid line, deconvolution curve; dash line, fitting curve.

also has been elucidated by thermal analyses of organoclays [21].

3.3.3. Br 3d spectra

As indicated by the survey scans of the resultant organoclays (Fig. 3), a very weak Br 3d transition begins to occur in the XPS spectrum of 1.5 CEC-Mt. The intensity of the Br 3d transition obviously increases in the spectra of 2.0 and 2.5 CEC-Mt. Fig. 6 displays the high-resolution Br 3d scans of HDTMAB, 2.0 and 2.5 CEC-Mt.

The Br 3d spectrum of HDTMAB displays two well-resolved transitions centered at 67.1 and 68.2 eV, corresponding to Br $3d_5$ and $3d_3$, respectively. In comparison to the XPS spectrum of HDTMAB, both 2.0 and 2.5 CEC-Mt shows a broad peak with low intensity and poor resolution for the two transitions. This reflects that the content of bromine in the organoclays is limited and disordered, and ion exchange between HDTMA$^+$ and interlayer cations (Na$^+$) is dominant [38].

3.3.4. O 1s and Si 2p spectra

The high-resolution O 1s scan of Na-Mt and the simulated curves (Fig. 7(a)) show that it is difficult to distinguish O and OH in montmorillonite. This is different from the previous study about basic aluminum sulphate and basic aluminum nitrate, in which O and OH in the corresponding materials were clearly identified [33]. There is a small amount of water (ca. 2.39%) remaining in Na-Mt after exposure to ultra high vacuum (10^{-9} to 10^{-10} Torr), as shown by the simulated curves (Fig. 7(a)). The oxygen in montmorillonite structural sheets corresponds to a binding energy of 532.1 eV while that in water is ca. 535.0 eV. These values are in accord with those reported in the literature [33,42]. However, the high-resolution O 1s scans of the resultant organoclays (Fig. 7) do not show any transition corresponding to H$_2$O, resulting from the hydrophobicity of the organoclays and high vacuum (10^{-9} Torr) in the detection chamber. Compared to Na-Mt, it can be seen that there is a slight decrease (ca. 1 eV) of the O 1s binding energy in the organoclays. The binding energy change of Si 2p transition from Na-Mt to the resultant organoclays is similar to that of O 1s (Fig. 7(d)–(f)). The binding energy of Si 2p in Na-Mt is 103.0 eV while that for the resultant organoclays increases to ca. 102 eV, with a decrease of ca. 1 eV. Both the decreases of O 1s and Si 2p binding energies result from the change of the interlayer environment. This is in agreement with the proposal deduced from MAS NMR study of organoclays, which indicates that modifying clays with surfactant results in a measurable shielding of ^{29}Si nuclei in clays [43].

During the intercalation, the prominent change for montmorillonite is that the exchangeable interlayer hydrated cations are
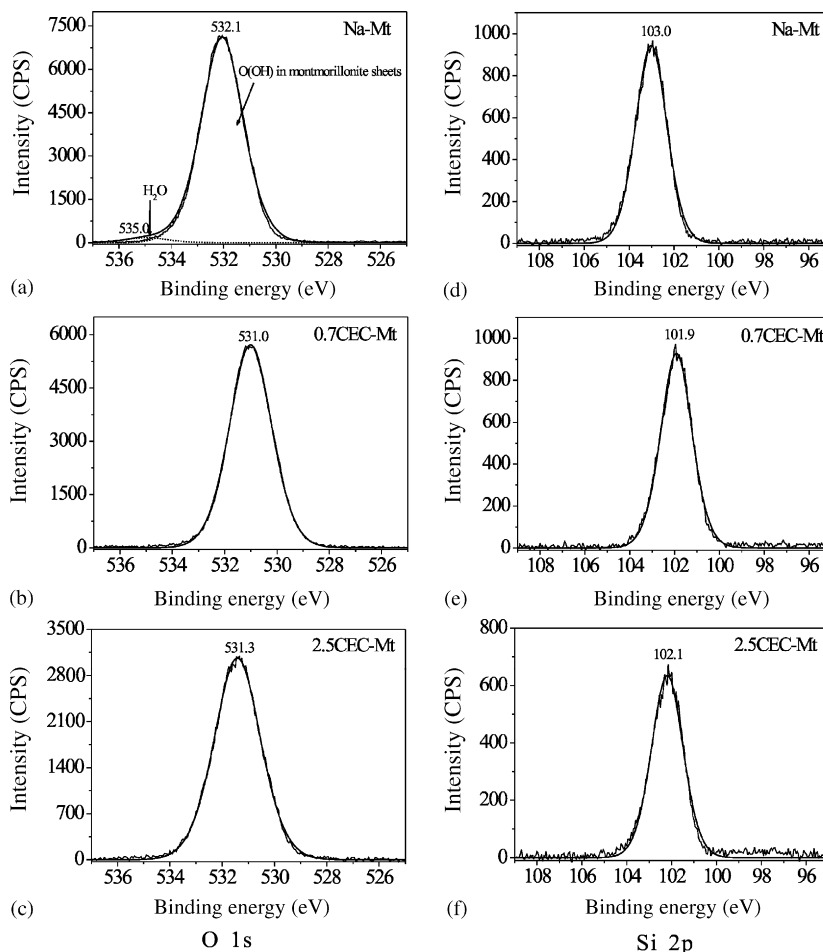

Fig. 7. O 1s and Si 2p high-resolution XPS spectra of Na-Mt and the representative organoclays. Thin solid line, experimental curve; thick solid line, deconvolution curve; dash line, fitting curve.

replaced by the surfactant cations. As shown by the O 1s XPS spectrum (Fig. 7(a)), there is a minor amount of H_2O in Na-Mt, corresponding to the strongly bound water of the interlayer cations rather than the surface adsorbed water [44,45]. This part of water links to the oxygen on the clay surface (Si–O tetrahedral sheet) through hydrogen bond [46,47]. After the interlayer hydrated cations are replaced by the intercalated surfactant, the main interaction between the clay and surfactant includes both the electrostatic attract between the positively charged head-groups (nitrogen) of the alkyl chains and the negatively charged clay surfaces, and a repulsive force between alkyl chain and clay surface as demonstrated by molecular modeling [34–36].

On the basis of above-mentioned experimental results, the schematics for the structural evolution from Na-Mt to the resultant organoclays are built as shown in Fig. 2(II). Obviously, two basic organoclay types are formed when modifying clay with surfactant due to the different surfactant distributions: (1) the surfactant mainly occupies the clay interlayer and (2) both the clay interlayer space and external surface are modified by surfactant. Our recent sorption experiments indicate that both surface sorption and partition are involved in the sorption mechanisms for 0.5, 0.7 and 1.0 CEC-Mt to p-nitrophenol, whereas partition is dominant for 1.5, 2.0 and 2.5 CEC-Mt. This is a convincing evidence supporting our assumption of the surfactant distribution within organoclays.

4. Conclusions

In this study, a series of organoclays with different surfactant arrangements within the clay interlayer were prepared. The surfactant distribution within the resultant organoclays was investigated by XPS in combination with XRD and HRTG. In the organoclays prepared at relative low surfactant concentrations (<1.0 CEC), the surfactant cations mainly occupy the clay interlayer with lateral arrangements (lateral monolayer, lateral bilayer and pseudotrilayer). However, when the surfactant concentrations are higher than 1.0 CEC, the surfactants occupy both the clay interlayer space and the interparticle pores, and paraffin type arrangements of surfactants (paraffin monolayer and paraffin bilayer) are adopted in the clay interlayer spaces. This finding could give excellent explanations about the dramatic pore volume decrease of organoclays and different sorption mechanisms (surface sorption and partition) involved in organoclay sorption experiments as reported in the literature.

XPS survey scans show that the peaks corresponding to magnesium and iron are identical in all samples, reflecting these atoms in montmorillonite structure rather in the interlayer or impurities. The peaks corresponding to bromine only appear in the organoclays prepared at high surfactant concentrations (>1.0 CEC). This suggests that both surfactant cations and ion pairs occur in these organoclays, corresponding to different interactions between surfactants and clays. The former relates with ion exchange and the latter with sorption.

Generally, modifying clays with surfactants results in a decrease of binding energy of atoms in both clays and surfactants and broadening of the peaks. However, with the increase of surfactant loadings, the FWHM of the related peaks decreases,

suggesting the organoclay structure becomes more ordered. This study shows that nitrogen is the most sensitive to the surfactant distribution within the resultant organoclays and the C 1s binding energy of C–C bond in alkyl chain is sensitive to the local environment of surfactants in organoclays with different arrangements.

References

[1] M.R. Stackmeyer, Appl. Clay Sci. 6 (1991) 39.
[2] L.P. Meier, R. Nueesch, F.T. Madsen, J. Colloid Interf. Sci. 238 (2001) 24.
[3] L.Z. Zhu, B.L. Chen, Environ. Sci. Technol. 34 (2000) 2997.
[4] L.Z. Zhu, B.L. Chen, X.Y. Shen, Environ. Sci. Technol. 34 (2000) 468.
[5] E. Manias, G. Hadziioannou, G. Brinke, Langmuir 12 (1996) 4587.
[6] Z. Wang, T.J. Pinnavaia, Chem. Mater. 10 (1998) 3769.
[7] S.S. Ray, M. Okamoto, Prog. Polym. Sci. 28 (2003) 1539.
[8] M. Nakatsuji, R. Ishii, Z.M. Wang, K. Ooi, J. Colloid Interf. Sci. 272 (2004) 158.
[9] R. Ishii, M. Nakatsuji, K. Ooi, Micropor. Mesopor. Mater. 79 (2005) 111.
[10] F. Bergaya, G. Lagaly, Appl. Clay Sci. 19 (2001) 1.
[11] G. Lagaly, Clay Miner. 16 (1981) 1.
[12] J.X. Zhu, H.P. He, J.G. Guo, D. Yang, X.D. Xie, Chinese Sci. Bull. 48 (2003) 368.
[13] R.A. Vaia, R.K. Teukolsky, E.P. Giannelis, Chem. Mater. 6 (1994) 1017.
[14] Y.Q. Li, H. Ishida, Langmuir 19 (2003) 2479.
[15] H.P. He, R.L. Frost, J.X. Zhu, Spectrochim. Acta A 60 (2004) 2853.
[16] H.P. He, R.L. Frost, Y.F. Xi, J.X. Zhu, J. Raman Spectros. 35 (2004) 316.
[17] Y.Q. Li, H. Ishida, Chem. Mater. 14 (2002) 1398.
[18] W. Xie, Z.M. Gao, W.P. Pan, D. Hunter, A. Singh, R.A. Vaia, Chem. Mater. 13 (2001) 2979.
[19] W. Xie, R.C. Xie, W.P. Pan, D. Hunter, B. Koene, L.S. Tan, R.A. Vaia, Chem. Mater. 14 (2002) 4837.
[20] S. Yariv, Appl. Clay Sci. 24 (2004) 225.
[21] H.P. He, Z. Ding, J.X. Zhu, P. Yuan, Y.F. Xi, D. Yang, R.L. Frost, Clay Clay Miner. 53 (2005) 287.
[22] H.P. He, R.L. Frost, F. Deng, J.X. Zhu, X.Y. Weng, P. Yuan, Clay Clay Miner. 52 (2004) 350.
[23] J.X. Zhu, H.P. He, L.Z. Zhu, X.Y. Weng, F. Deng, J. Colloid Interf. Sci. 286 (2005) 239.
[24] S.Y. Lee, S.J. Kim, Colloid Surf. A 211 (2002) 19.
[25] S.Y. Lee, S.J. Kim, Clay Clay Miner. 50 (2002) 435.
[26] Y.M. Dana, C. Yona, N. Shlomo, P. Rene, Environ. Sci. Technol. 29 (2005) 1231.
[27] T.N. Wittberg, P.S. Wang, Surf. Interf. Anal. 27 (1999) 936.
[28] G. Parthasarathy, B.M. Choudary, B. Sreedhar, A.C. Kunwar, R. Srinivasa, Am. Mineral. 88 (2003) 1983.
[29] J.X. Du, J. Zhu, C.A. Wilkie, J.Q. Wang, Polym. Degrad. Stabil. 77 (2002) 377.
[30] M. Bueno, A. Astruc, J. Lambert, M. Astruc, P. Behra, Environ. Sci. Technol. 35 (2001) 1411.
[31] H.P. He, J. Duchet, J. Galy, J.F. Gérard, J. Colloid Interf. Sci. 295 (2006) 202.
[32] H.P. He, J.G. Guo, X.D. Xie, J.L. Pen, Environ. Int. 26 (2001) 347.
[33] L.V. Duong, B.J. Wood, J.T. Kloprogge, Mater. Lett. 59 (2005) 1932.
[34] P. Čapková, J.V. Burda, Z. Weiss, H. Schenk, J. Mol. Model. 5 (1999) 8.
[35] Q.H. Zeng, A.B. Yu, G.Q. Lu, R.K. Standish, J. Phys. Chem. B 108 (2004) 10025.

[36] H.P. He, J. Galy, J.F. Gerard, J. Phys. Chem. B. 109 (2005) 13301.
[37] L. Bugyi, A. Oszkó, F. Solymosi, Surf. Sci. 461 (2000) 177.
[38] Z. Klapyta, T. Fujita, N. Iyi, Appl. Clay Sci. 19 (2001) 5.
[39] A.N. Buckley, M.D. Kelly, P.F. Nelson, K.W. Riley, Fuel Process. Technol. 43 (1995) 47.
[40] G. Lagaly, S. Ziesmer, Adv. Colloid Interf. 100 (2003) 105.
[41] D. Burgentzlé, J. Duchet, J.F. Gérard, A. Jupin, B. Fillon, J. Colloid Interf. Sci. 278 (2004) 26.

[42] T.L. Barr, M.A. Lishka, J. Am. Chem. Soc. 108 (1986) 3178.
[43] I.K. Breakwell, J. Homer, M.A.M. Lawrence, W.R. Mcwhinnie, Polyhedron 14 (1995) 2511.
[44] A.F.K. van Groos, S. Guggenheim, Am. Mineral. 72 (1987) 292.
[45] Y.F. Xi, R.L. Frost, H.P. He, J.T. Kloprogge, T. Bostrom, Langmuir 21 (2005) 8675.
[46] L. Yan, C.B. Roth, P.F. Low, Langmuir 12 (1996) 4421.
[47] L. Yan, P.F. Low, C.B. Roth, Clay Clay Miner. 44 (1996) 749.